Spaceborne C-band SAR remote sensing–based flood mapping and runoff estimation for 2019 flood scenario in Rupnagar, Punjab, India

Akshar Tripathi ⓘ · **Luvkesh Attri** ⓘ ·
Reet Kamal Tiwari ⓘ

Abstract   Floods are one of the most disastrous and dangerous catastrophes faced by humanity for ages. Though mostly deemed a natural phenomenon, floods can be anthropogenic and can be equally devastating in modern times. Remote sensing with its non-evasive data availability and high temporal resolution stands unparalleled for flood mapping and modelling. Since floods in India occur mainly in monsoon months, optical remote sensing has limited applications in proper flood mapping owing to lesser number of cloud-free days. Remotely sensed microwave/synthetic aperture radar (SAR) data has penetration ability and has high temporal data availability, making it both weather independent and highly versatile for the study of floods. This study uses space-borne SAR data in C-band with VV (vertically emitted and vertically received) and VH (vertically emitted and horizontally received) polarization channels from Sentinel-1A satellite for SAR interferometry-based flood mapping and runoff modeling for Rupnagar (Punjab) floods of 2019. The flood maps were prepared using coherence-based thresholding, and digital elevation map (DEM) was prepared by correlating the unwrapped phase to elevation. The DEM was further used for Soil Conservation Service-curve number (SCS-CN)-based runoff modelling. The maximum runoff on 18 August 2019 was 350 mm while the average daily rainfall was 120 mm. The estimated runoff significantly correlated with the rainfall with an R^2 statistics value of 0.93 for 18 August 2019. On 18 August 2019, Rupnagar saw the most devastating floods and waterlogging that submerged acres of land and displaced thousands of people.

Introduction

The phenomenon of a flood is the most common and one of India's most devastating natural disasters (Gupta et al., 2003). Floods are a yearly and common feature in the Gangetic and Brahmaputra plains and lead to huge loss of life and property. Apart from this, floods render millions of people homeless, cause food shortage, and waterlogging that often leads to widespread epidemics (Phalkey et al., 2012). Apart from this, floods cause the failure of cities' drainage systems, disruption of the telecommunications network, and widespread submergence of precious agricultural and forest land. All this causes a considerable loss for the country's economy

A. Tripathi · L. Attri · R. K. Tiwari (✉)
Department of Civil Engineering, Indian Institute
of Technology (IIT) Ropar, Rupnagar 140001-Punjab,
India
e-mail: reetkamal@iitrpr.ac.in

A. Tripathi
e-mail: 2018cez0004@iitrpr.ac.in

L. Attri
e-mail: 2017ceb1013@iitrpr.ac.in

(Kale et al., 1994). Since ages, floods have been a naturally occurring event, caused due to heavy rainfalls, glacial lake outbursts, and cloud bursts. With increased human intervention in the surrounding environments, the causes of floods became anthropogenic (Sanyal & Lu, 2005). If losses due to floods are to be reduced, the aim should be to predict, model, map, and prepare a reliable database on a yearly and decadal basis. This would help to study floods, and mark out flood-prone and low-lying areas (Mishra et al., 2010).

With the advent of remote sensing, it is now possible to have reliable and accurate maps that help in relief measures and relocate populations dwelling in flood-prone and low-lying regions (Jayraman et al., 1997). Remotely sensed data is also utilized to mark out the weak canal linings that could be repaired before the monsoon season. But optical remote sensing, mainly the multi-spectral remote sensing data used so far, does not have an all-weather availability (Peters et al., 2012) and thus, microwave remote sensing or SAR data was brought into use.

Topological characters, and different soil types with land use as hydrological soil group, have been essential for runoff studies. Further, surface runoff has often been dependent on the climatic, geomorphological, topological, and land use/land cover (LULC) features of a catchment area or watershed (Mishra & Singh, 1999). Combining the characteristics which are favorable for the runoff generation and concentration of runoff leads to an increase in the flood potential of a watershed (Amutha & Porchelvan, 2009). Most Indian watersheds are poorly gauged or at times ungauged, as there is a paucity of records for runoff generation for a rainfall or flash flood event to understand hydrological response (Mishra et al., 2004). It is crucial to calculate peak flood discharge or flood potential of each watershed in a flood-affected catchment. Several methods are used for discharge estimation—the rational method, Soil Conservation Service-curve number (SCS-CN) method, Cook's method, and the unit hydrograph method (Mishra et al., 2008).

However, the most important and commonly used is the SCS-CN method for predicting runoff or discharge from rainfall events in ungauged watershed areas (Geetha et al., 2008). This method is robust and facilitates the delineation and watershed zoning in areas with a high risk of re-occurring floods, and for areas exposed to large volumes of runoff generations. Along with the soil, the LULC parameters control

the surface runoff and are evaluated and mapped with high accuracy using various remote sensing satellite imageries (Nishida et al., 2003). Research conducted by Sharma and Singh (2015) successfully utilized Landsat TM data to estimate the runoff potential of the Luni river basin using the SCS-CN method. Another study conducted by Katimon et al. (2003) utilized remote sensing data from Landsat TM and Geographical Information System (GIS) for runoff modeling of two watersheds in the Selangor and Pontian of Malaysia using the same method successfully. It generated a relationship between rainfall and runoff. However, it was found that the SCS-CN method though highly robust yet, suffers from a limitation that it needs hydrological soil group data for accuracy. Large variations in runoff and rainfall relationships were reported in the event of a change in soil group.

A study that used the SCS-CN method for runoff modeling of the Tarik basin of Iran was conducted by Behzad et al. (2012) as cited by Sharma and Singh (2014). However, the study concentrated more on the geomorphological properties of the area. The reliability of the parameters largely varied between the various methods, and none of them were found to be suitable. Despite few limitations in the SCS-CN method, with hydrological soil group, and LULC information, it remains a widespread flood potential estimating technique for the poorly gauged and ungauged catchment areas owing to its robustness and accuracy.

Changing monsoon trends: fewer rainy days but more rainfall

Climate change and increased anthropogenic interference like clearing of forest lands (Bronstert, 2003) and construction of megastructures are causing changes in rainfall trends worldwide, and India is no exception (Revi, 2008). While this is leading to increased desertification in few areas, and on the other hand, is causing unprecedented floods in different regions (Sivakumar, 2007). The 2013 floods in Kedarnath valley stand testimony of how the sudden excess rains due to cloud bursts and glacial lake outflows can cause devastation down the valley slopes (Ahluwalia et al., 2016). Over the years, flash floods have become a significant catastrophe in Indian Himalayan region where despite the fewer number of rainy days, there have been excessive and

sudden rainfalls recorded (Kumar et al., 2018). The recent floods that happened in the Indian state of Kerala in 2019 is a fresh example of this and what is more serious is that no or inadequate rainfall during cropping months can delay sowing of crops and sudden downpour causes submergence of large chunks of agricultural lands (Saini et al., 2020). In recent years, there have been flooding events in arid and semi-arid regions of Rajasthan in India all due to sudden and excessive rainfalls. Such rainfalls often cause drainage problems and high surface runoff. Similar events are being recorded the world over, and a recent example from Egyptian drylands is a fresh example recorded by Abdeldayem et al. (2020). On analyzing the trends in the Indian rainfall scenario, the difference between the mean and median rainfall is increasing significantly. Since the last and current decade of this century, the mean rainfall and median rainfall difference are much more than the difference in five decades of the previous century (Alexander & Arblaster, 2009; Hughes, 2000). When most of the season is dry, the middle value of rainfall is called the median value, and it becomes more significant when there is a sudden burst of rainfall for a few days. The analysis window must be narrowed down for a more detailed study of rainfall variations (Heino et al., 1999). With more availability of satellite data with a high temporal resolution, it is easy to utilize space-borne remote sensing to study and analyze the rainfall trends that are changing abruptly and the causative factors behind them. Sentinel-1 has a 12-day repeat pass and is exceptionally helpful for mapping and monitoring flood events. Its high spatial resolution can help runoff estimation for smaller regions in shorter periods, as used in this study.

Strength of Sentinel-1A, C-band SAR data for flood inundation mapping

Floods worldwide, mostly are rain-induced or occur in rainy seasons when there is dense cloud cover (Kuenzer et al., 2013). Hence, optical remotely sensed data is not feasible for flood mapping and runoff estimation as it is opaque to cloud cover (Tripathi & Tiwari, 2020). SAR data with its penetration abilities and weather independence is highly feasible for remote sensing analysis in rainy seasons (Kuenzer et al., 2011; Tsai et al., 2019). SAR data applications include crop monitoring, flood mapping, and runoff estimation

and modelling. Since floods are a highly dynamic phenomenon and runoff is a short span event; hence it becomes more critical to have remotely sensed SAR data with a high temporal resolution (Clauss et al., 2018; Sanyal & Lu, 2004). Sentinel-1 has a repeat pass of 12 days and a spatial resolution after multi looking close to 14 m. Thus, it is highly feasible for a high-resolution interferometric DEM generation and a coherence-based flood inundation mapping irrespective of how dense the cloud cover over an area (Chini et al., 2019). The high-resolution DEM can be used for a time-saving runoff estimation. Moreover, as this data is freely available, it makes the study time-saving and cost-effective (Sanyal & Lu, 2004).

Of the many studies conducted for flood inundation mapping using Sentinel-1 SAR data, a study conducted by Borah et al. (2018) is noteworthy. It utilized Sentinel-1 SAR data and threshold-based backscattering for flood inundation mapping for Kaziranga National Park in Assam, India. The constraint with optical data in this context was the dense cloud cover and limited cloud-free data availability. A similar study was conducted using Sentinel-1 SAR Interferometry and coherence-based thresholding to map the flooded regions for Gorakhpur floods of Uttar Pradesh in India by Tripathi and Tiwari (2019a). Sentinel-1 SAR data is highly feasible for flood mapping globally owing to its weather independence, high temporal data availability, and high spatial resolution, as extensively reviewed by Shen et al. (2019). The high temporal resolution of Sentinel-1 SAR data increases the chance of data availability on the day of flood occurrence. A recent study conducted for flood inundation mapping for Pakistan by Zhang et al. (2020) also establishes Sentinel-1 C-Band SAR data, as a highly robust and potent tool for flood mapping.

SCS-CN method and its applicability in the Indian context

Though developed initially for the USA, the SCS-CN method has evolved over the years as a robust and widely used technique for runoff estimation. It has been proved by the many studies carried out successfully using the SCS-CN technique all over the world, including India. However, since it is an analytically developed technique, with varying watersheds and different soil types than mentioned in the US Geological Survey (USGS) soil groups, the method needs certain empirical modifications

to explain when surface retention "S" equals the peak maximum accumulation "F." Mishra and Singh (1999) suggested a modification in the SCS-CN technique. However, in most cases, the method can be applied in its raw form and has given encouraging results as shown by the studies conducted by Ramakrishnan et al. (2009) to estimate the runoff for Kali watershed of the Mahi river. The study assessed the surface runoff successfully and suggested the means and measures to arrest this runoff by constructing infiltration trenches so that increasing desertification problems and groundwater table lowering problems could be minimized.

A noteworthy study for runoff estimation modeling was conducted by Satheeshkumar et al. (2017), where the authors mentioned the constraint in the technique for a large area with heterogeneous soil type (based on grain size, porosity, and other soil properties). For smaller areas under study and with similar soil types over an extensive watershed, the SCS-CN method becomes easy, robust, and time-saving. Geetha et al. (2007) utilized the SCS-CN method for runoff estimation for Hemavati watershed in Karnataka, India. The study observed that when the antecedent moisture condition is replaced with antecedent moisture condition amount, the efficiency of the technique improved over large watersheds and is highly feasible for large-scale hydrological simulations. Latha et al. (2012) compared the SCS-CN method with the field-based strange table method used by the Tamil Nadu irrigation department to estimate surface runoff. The study found that the SCS-CN method performed better and more efficiently than the strange table method used earlier. Despite some limitations and constraints like varied soil types, a larger area under watershed, and different watershed types, the SCS-CN method has been applied successfully in Indian contexts for different regions in an efficient manner (Amutha & Porchelvan, 2009; Kadam et al., 2012).

In August 2019, flash floods in Rupnagar district and many other districts of Punjab were observed due to cloud bursting in Himachal Pradesh. It was found that there is an abrupt variation in the correlation between rainfall and runoff on 18 August 2019 in Rupnagar when despite being average rainfall, the runoff was high. It led to waterlogging in large parts of the district and submerged acres of precious agricultural land and displacing thousands of people. It was an abnormal situation that occurred due to cloud bursting events high up in the Himalayas that caused Sutluj river waters to swell up beyond the critical marks.

This study relies mainly upon the SAR data from Sentinel-1 A for runoff modelling and coherence-based flood mapping. The study aims to establish the versatility of SAR data and does not use optical datasets at all. The study is cost-effective since freely available DEM has a coarser spatial resolution (up to 30 m for ASTER DEM). This study uses dual polarized SAR data with VV and VH polarization channels for 14 m DEM generation using interferometric processing (InSAR). The rest of the procedure is in with the SCS-CN method. SCS-CN method was used in this study due to its simplicity, efficiency, and reliability, which was found after a rigorous literature survey. The method development dates to 1954 which has been well documented in Sect. 4 of National Engineering Handbook (NEH), published by the SCS now (since 1956) called the National Resource Conservation Service of the United States Agriculture Department (Mishra & Singh, 2004).
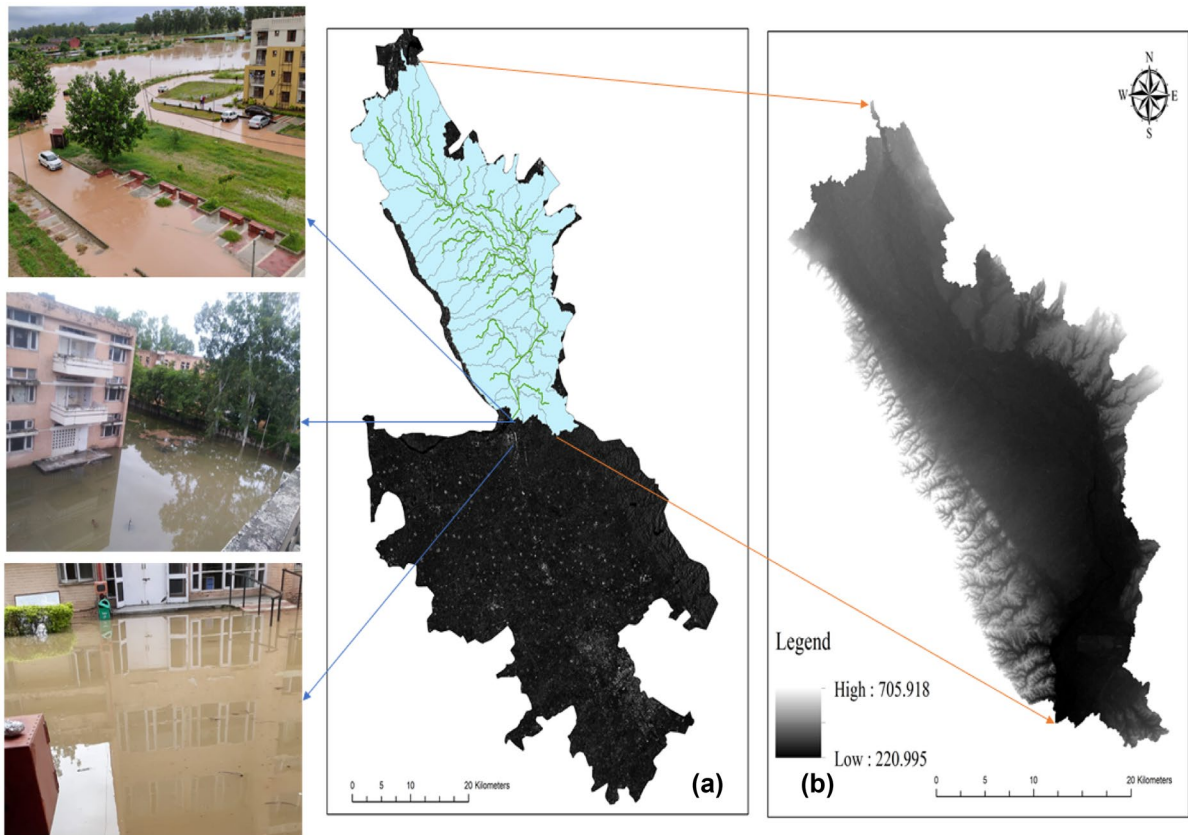
Study area

The study area chosen for this study is the Rupnagar watershed which is in the Rupnagar district. Rupnagar is a district of Punjab state in India and one of the sites of Indus Valley Civilization (Wright, 2009). Today Rupnagar is located on the river Sutlej banks and the foothills of mighty Shivalik hills of the lofty Himalayas. As it is well known, Punjab is the cradle of India's first green revolution and for decades dominated the wheat production in the country owing to its vast canal network and mechanized agricultural practices (Damodaran, 2008). Rupnagar is no exception to this. It has lush green agrarian fields with wheat and sugarcane being significant crops. Rupnagar is located at 30.97° N, and 76.53° E with an average elevation of 260 m above mean sea level. Figure 1 shows the Sentinel-1A imagery of the study area.

Materials and methods

Materials

Slant range Single Look Complex (SLC) datasets from Sentinel-1A, for August 6, 18, and 31 for the year 2019 of Rupnagar area was used for this study. The rainfall

Fig. 1 (**a**) Sentinel-1 SAR imagery with Rupnagar watershed draped over and field photographs of flood scenario of the study area. (**b**) DEM map of Rupnagar watershed with elevation in meters

data for August 2019 over Rupnagar was used from the CHRS data portal (https://chrsdata.eng.uci.edu/).

Sentinel-1A is a RADAR imaging satellite of the European Space Agency (ESA) onboard the Copernicus mission (Bézy et al., 2014). It was launched in February 2014 and had since been providing all-weather, day, and night data with global coverage and a 12-day repeat pass. This satellite data has been extensively used for coastal landform monitoring, ship detection, sea-routes monitoring (Zhu et al., 2018), LULC change and modeling, Flood mapping, and archaeological applications. It has a primary operation mode over landmasses and a separate over the ocean, which provides a conflict and error-free data acquisition. The primary operational mode offers it a large swath of 250 km and 20 m spatial resolution for Level-1 product and a high radiometric resolution (Tapete, 2018).

For this study IW product (since it is the standard Sentinel-1 product overland) of 20 m, spatial resolution was taken. Since the Sentinel-1 IW product has different spatial resolutions in range and azimuth directions, it was necessary to generate square pixels. For generating square pixels, space domain averaging was done, and the process is termed multi looking. It resulted in an image with 14 m spatial resolution.
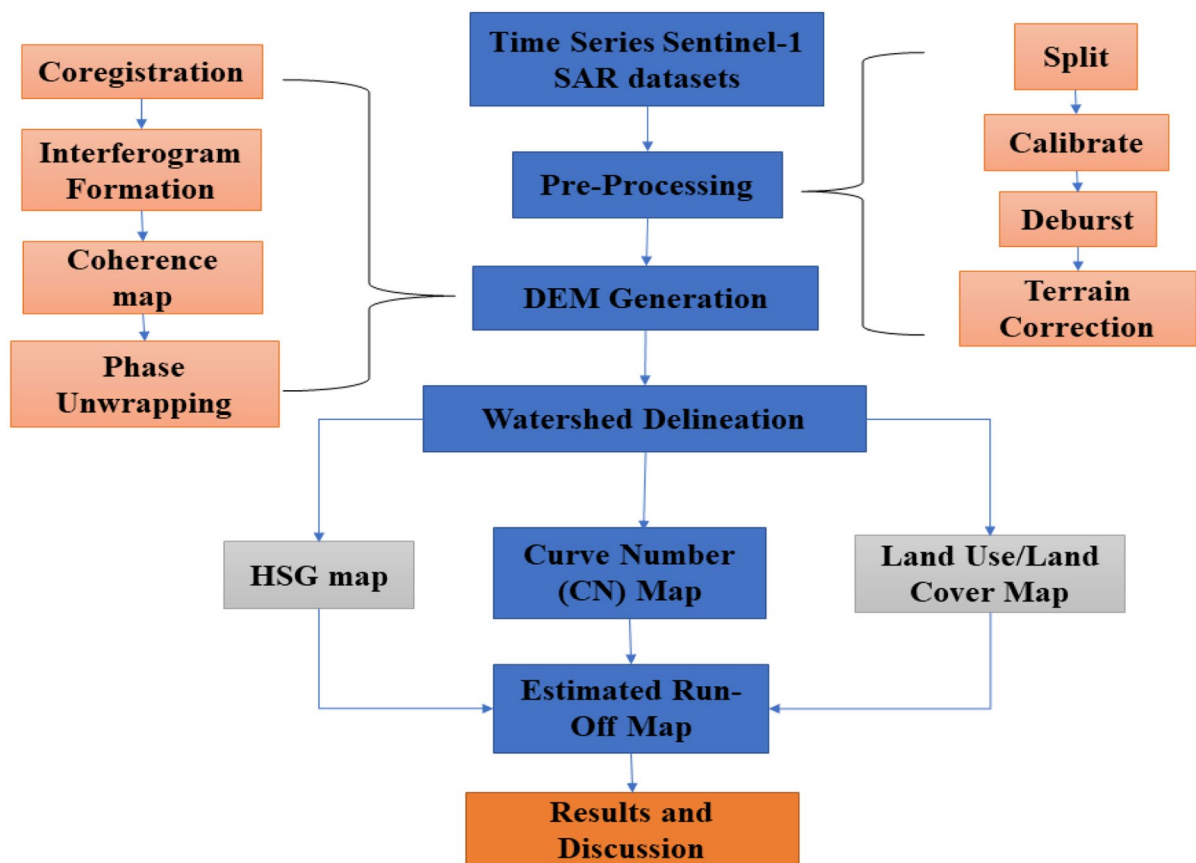
Methods

Time series Sentinel-1A, C-band SAR datasets were taken and pre-processed followed by interferometric processing for DEM generation. Based on the DEM map, the Rupnagar watershed was delineated and was utilized for runoff estimation. The detailed methodology flowchart is shown in Fig. 2.

DEM generation

The microwave datasets were in interferometric wide (IW) tile format; hence, to delineate the study area, it had to be split first before further processing. This also removed any residual radiometric distortions in the imagery (Tripathi & Tiwari, 2019a). Followed by this, since the datasets were acquired in burst or scan mode, it had to be deburst to remove any RADAR distortions. Therefore, calibration of the datasets was done to generate pure backscatter signals from different features—single bounce from smooth surfaces, double bounce from urban and built-up, and volumetric from trees and vegetation. For the generation of square pixels of 14 m × 14 m size, since the data has a different spatial resolution in range and azimuth directions, multilooking was performed (Xu & Jin, 2007). Following this, the data co-registration was conducted date wise where earliest date data was

taken as a master image and rest as slave images, and their pixels were aligned to the master image. For correlating the image with the actual ground coordinates, the image was orthorectified in a process known as terrain correction using World Geodetic System (WGS) 1984 as the projection system (Grandin et al., 2016). This was followed by the interferometric processing, in which the phase variations and amplitude distortions that occur in backscattered waves throughout the study are analyzed to phase and amplitude values of the master image (Lanari et al., 1996; Sandwell & Price, 1998).

After this, the interferometric phase and amplitude were observed for changes. Interferogram generation is achieved by the multiplication of the master image used in co-registration with the complex conjugate of itself (Tripathi & Tiwari, 2019b). Here, the phase change in the backscattered signal received, and the emitted wave from the sensor were analyzed (Lloyd, 1987). Regularity

Fig. 2 Methodology flow diagram for runoff estimation

in the interferogram fringes shows flatness in the land area, while irregular ones show a topography change (Naab et al., 2013). Persistent scatterers like built-up features show a high value of coherence (close to 1) between original and backscattered signals as they do not tend to vary over time (Frederick et al., 1986). The coherence maps generated from the interferogram were analyzed for loss of coherence from persistent Scatterers due to any water accumulation as permanent features tend to show high coherence value (close to 1) compared to dynamic features like soil and vegetation that loose coherence very quickly (Tripathi & Kumar, 2019).

The phase wrap ambiguity occurs when an interferogram wraps each time to value of 2π is removed. The phase unwrapping is done to remove the 2π phase ambiguity in the interferogram, which renders an unwrapped phase. From the unwrapped interferometric phase, the phase information is related to elevation. It is done by removing all the integer number of amplitudes of ambiguity (equivalent to an integer number of 2π phase cycles). The time-scale variation in phase, between two different points on flattened interferogram, gives a measurement of the actual variation of altitude, which is then used for a phase to elevation relation for DEM generation (Chung et al., 2015; Dongchen et al., 2004).

The phase formula is given as follows (Cosgrove & Loucks, 2015; Tripathi & Tiwari, 2019c):

$$\varphi 1 = 4\pi R/\lambda \tag{1}$$

$$\varphi 2 = (R + dR)/\lambda \tag{2}$$

$$
\begin{aligned}
d\varphi i, k(s,l) &= \varphi 2i(s,l) - \varphi 1k(s,l) \\
&= \textit{Interferrometric phase difference} \\
&= 4\pi(dR)/\lambda
\end{aligned} \tag{3}
$$

where R is the satellite target distance, and φ is the phase. The interferogram formula is as follows (Jung et al., 2016)-

$$Int_{i,k}(s,l) = Img_i(s,l).Img_k(s,l)^* \tag{4}$$

where "i" and "k" are master and slave images, respectively, $(s,l)^*$ represents the complex conjugate. After that, a coherence map was obtained since coherence shows the similarity between master and slave images. Usually, urban and built-up areas show high values of coherence, close to 1. However, there was a considerable loss of coherence in and around the areas located near the river and the lake in the city core in this study. Only the areas at a higher elevation, show a high value of coherence. The coherence varies typically between 0 and 1. The interferometric coherence equation is as follows (Boerner, 2007):

$$\gamma i, k = \frac{E[imgi.imgk^*]}{\sqrt{E[imgi]^2 E[imgk^*]^2}} \tag{5}$$

where "i" and "k" represent the master and slave images, respectively.

Phase to height conversion for DEM generation is done by the following formula (Small et al., 1996):

$$\Delta h = \frac{\lambda.r1.sin\theta}{4\pi.Bn}.\Delta\phi \tag{6}$$

where r_1 is the slant range in the first image, B is the normal component to the baseline, λ is the radar wavelength, and θ is the incidence angle. The above relationship is used to integrate across the image, transforming from phase to height values. The model's accuracy suffers from using only a single normal baseline value for all heights at the same slant range. The generated DEM map for the Rupnagar watershed is shown in Figs. 1b and 4a.

Runoff modelling

Watershed delineation

A digital elevation model (DEM) of 15 m raster cell size has been used to delineate watershed for the Sutlej river basin around Rupnagar North using BASIN hydrological model (Murmu et al., 2019). The steps were followed as follows: (i) create a depression less DEM; (ii) calculation of the flow direction based on 3×3 cell neighborhood; (iii) calculation of the flow accumulation and identification of cell having given area under study; (iv) watershed delineated outlet points leading to the delineation of watersheds for the given threshold area. The watershed area was calculated to be 700.49 km^2. The Rupnagar watershed is shown in Fig. 1a.

LULC map

A LULC map was prepared by classifying the Sentinel-1A imagery using artificial neural network classifier with 93% overall accuracy and kappa coefficient of 0.92. The LULC map for Rupnagar watershed is shown in Fig. 3.

HSG Map

For the generation of hydrological soil group (HSG) maps, a comparison of the soil types was done with the soil texture map obtained from a soil survey of India. Soil properties were then identified, and a GIS map for HSG was prepared. The HSG map gives an idea of the soil infiltration properties of an area and the overall drainage. The soil group B here refers to the rate of moderate infiltration and well-drained to moderately drained soil. The soil group C here refers to soils with moderately fine to rough textures and moderate rates of transmission. When combined with the LULC map of the watershed, the HDG Map helps to find the runoff curve number, as shown in Fig. 4b.

CN map generation

CN value denotes the maximum soil retention value of an area. A value of CN = 100 denotes an impervious surface while a value of 0 denotes a highly pervious surface (Pandit & Heck, 2009). The value varies from 0 to 100. Based on the curve number, the maximum potential storage varies with the LULC of the area, the HSG properties of the soil, and the hydrological conditions.

CN plugin of ArcGIS Hydro was used in this study for the CN map generation for the Rupnagar watershed. For vector intersection, HSG map and LULC map of the watershed as shown in Fig. 4, were used (Mishra et al., 2008). After the intersection, curve numbers were assigned to each polygon of the resulting CN map as shown in Fig. 4c.

The runoff CN is an empirical parameter that is used for the estimation of runoff or infiltration from an excess of rainfall. Low values of CN indicate a low runoff potential, while higher values indicate a higher potential for the runoff. A lower curve number indicates a highly permeable soil. As inferred from Fig. 4c, runoff begins after the initial abstraction value has been met that is the minimum CN value for a watershed. The CN is based on event rainfall and cannot be used for single annual rainfall value which misses antecedent moisture conditions that are needed in this technique for runoff estimation. Figure 4d shows the flooding in the southern direction of the watershed in and around the Indian Institute of Technology Rupnagar campus. The reason being that runoff follows the natural slope of the terrain and flood being an outpour event of a runoff, occurs where there is flat land and water can accumulate. Table 1 shows the contribution of LULC categories to runoff contribution-

Comparing the data given in Table 1, with the estimated runoff map, the land use category contributing to the maximum runoff can be inferred.

Estimation of runoff

An assumption made with the SCS-CN method is that the surface runoff is generated after compensating and minimization of the losses. SCS-CN water balance equations are as follows (Cheng et al., 2006). Here, it is assumed that the direct runoff and rainfall depth ratio minus the initial losses equals the cumulative infiltration-

$$P = Q + F + Ia \tag{7}$$

$$\frac{P}{Q - Ia} = \frac{F}{S} \tag{8}$$

where P is the total rainfall in mm, I_a represents the initial abstraction in mm, Q is a runoff in mm, S is the maximum retention or the storage capacity of the soil. According to the USDA-SCS Guidelines of 1985 as mentioned by Boughton (1989), the abstraction initially is assumed in terms of the fraction of maximum retention (usually, $\lambda = 0.2$) (Wałęga & Rutkowska, 2015).

$$I_a = \lambda S \tag{9}$$

The runoff Q_p is related to the maximum precipitation and the maximum retention by soil using the water balance equation, assuming $I_a = 0.2S$ (Wałęga & Rutkowska, 2015)–

$$Q_P = \frac{(P - Ia)2}{(P - Ia + S)} = \frac{(P - 0.2S)2}{(P + 0.8S)} \tag{10}$$
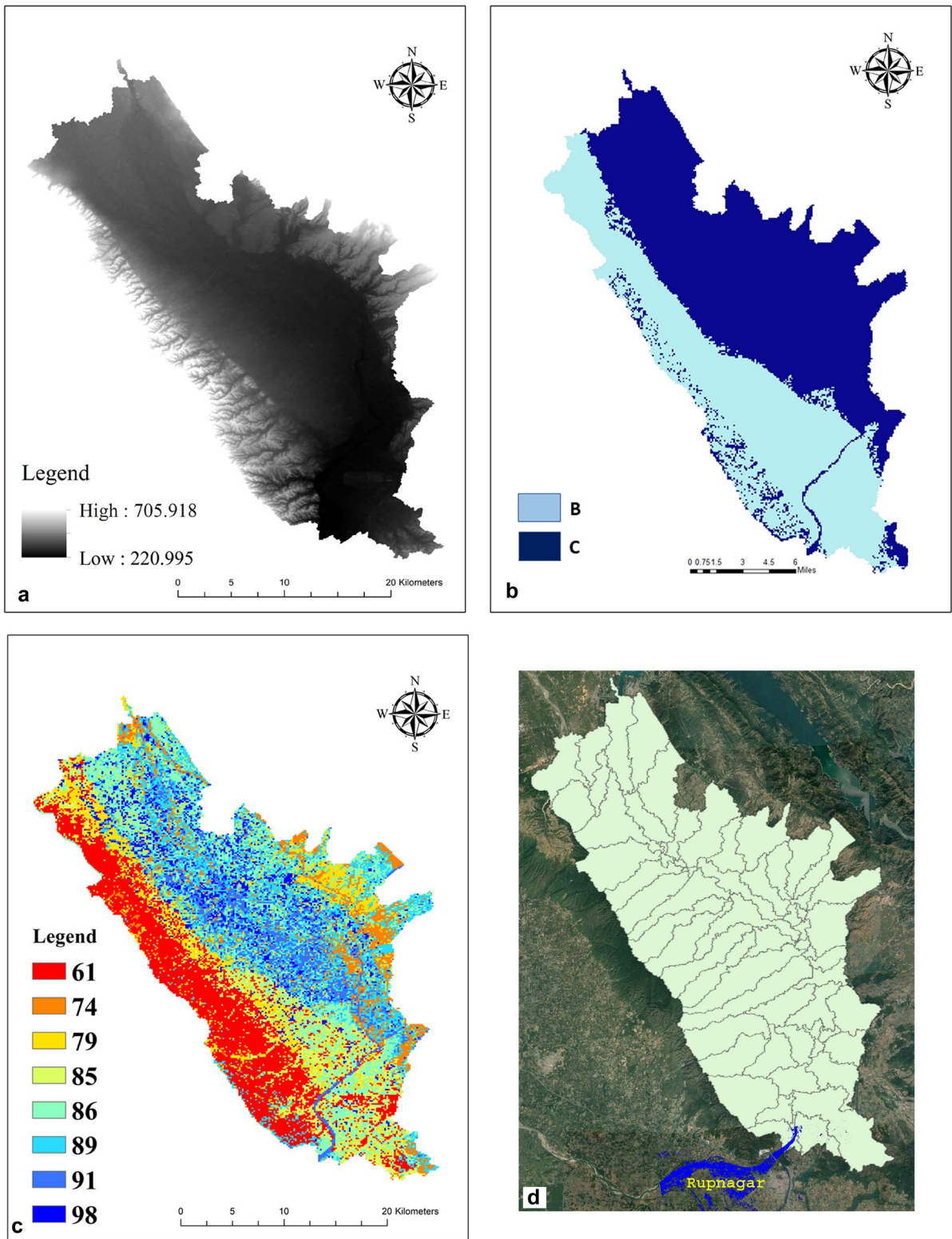
If the effective rainfall $P < \lambda$ S, then the effective runoff is assumed to be zero. The potential maximum retention S is obtained from curve number CN using the following equation (Hoomehr et al., 2013).

$$S = \frac{254400}{CN} - 254 \tag{11}$$
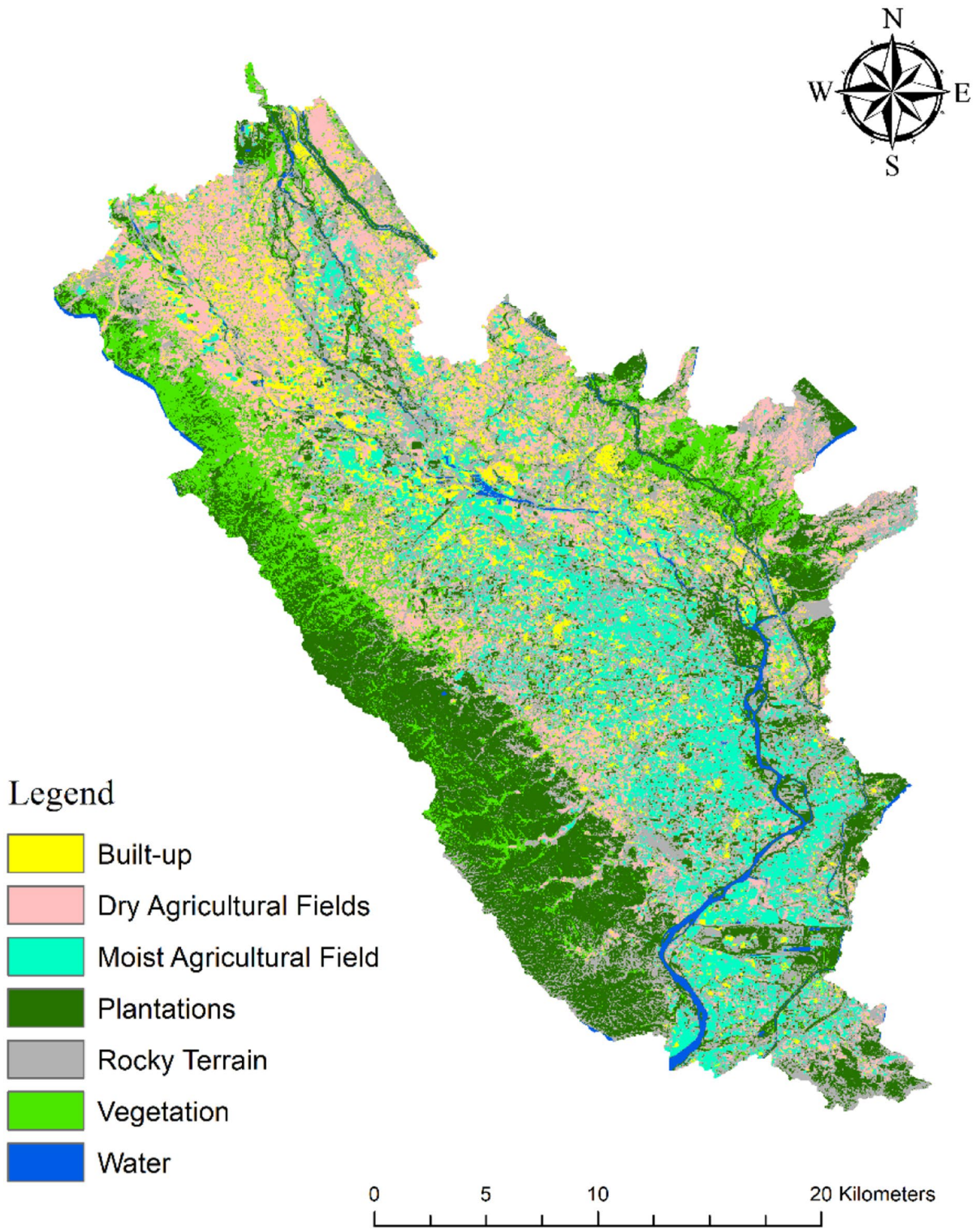
Fig. 3 LULC map of Rupnagar

Fig. 4 a DEM of Rupnagar watershed. **b** HSG map of Rupnagar watershed. **c** CN II map of Rupnagar watershed. **d** Flood inundation map (Rupnagar city) for 18 August 2019 with Rupnagar watershed

Table 1 Distribution of curve numbers (CN), land use categories, and hydrological soil group

Land use	HSG	CN	Area (km^2)
Built-up	B	86	10.4
	C	89	60.09
Dry agricultural fields	B	89	6.03
	C	96	50.21
Moist agricultural fields	B	86	80.12
	C	79	200.07
Plantations	B	74	100.08
	C	61	26.02
Rocky terrain	B	74	45.02
	C	89	55.05
Vegetation	B	74	12.21
	C	79	30.15
Water	B	91	1.01
	C	96	20.3

The CN is obtained from a table based on land use, HSG of soil, and antecedent moisture condition (AMC). Based on the infiltration of soil, HSG has four categories A, B, C, and D while AMC has four classes as I, II, III, and IV based on precipitation for sowing and crop growth seasons (Schwartz, 2010). Since the runoff inputs (rainfall, peak retention, etc.) were in millimeters (mm), the SCS-CN method gives the runoff in mm as well in terms of equivalent of standing water and not in terms of volume (Soulis & Valiantzas, 2012). The estimated runoff was correlated with the rainfall data from the CHRS data portal, as shown in Fig. 6.
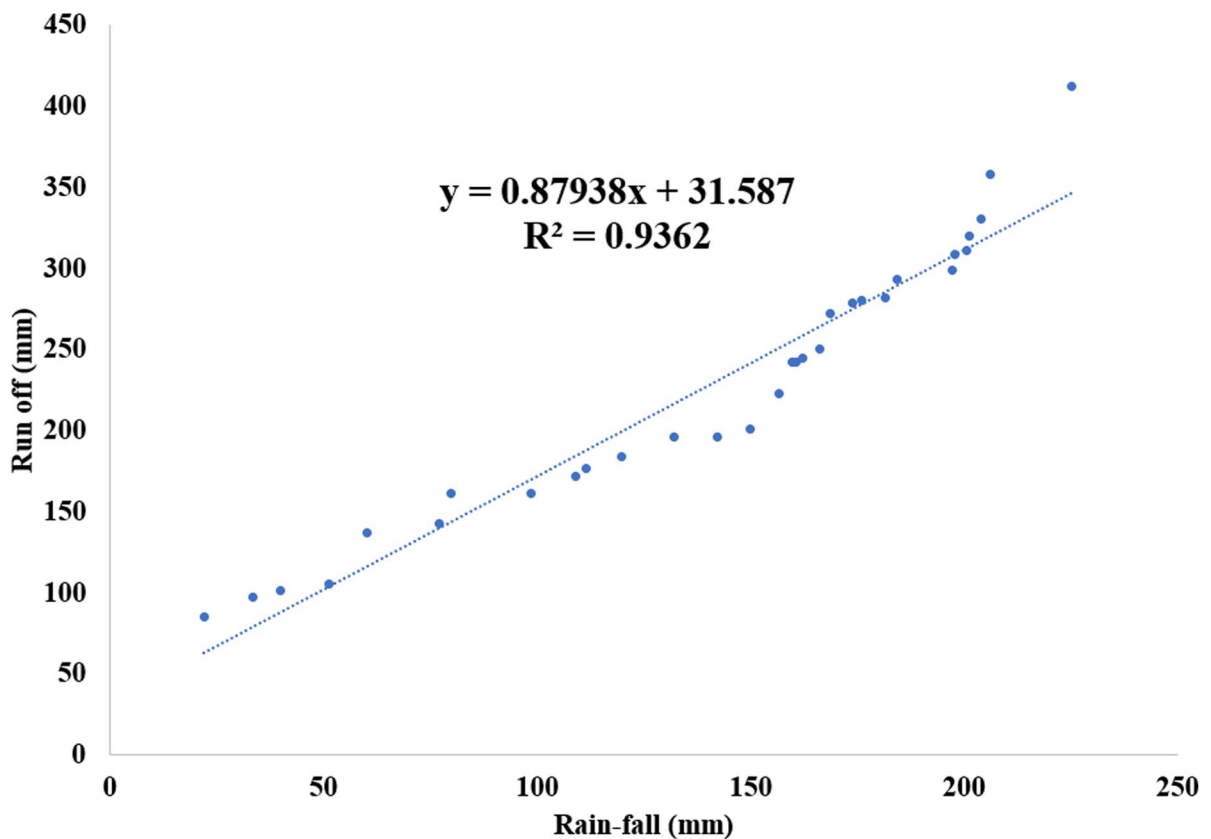
The flood map

Since the areas with persistent Scatterers in InSAR data show a high degree of coherence, mainly from built-up areas, but in flood events, these areas are
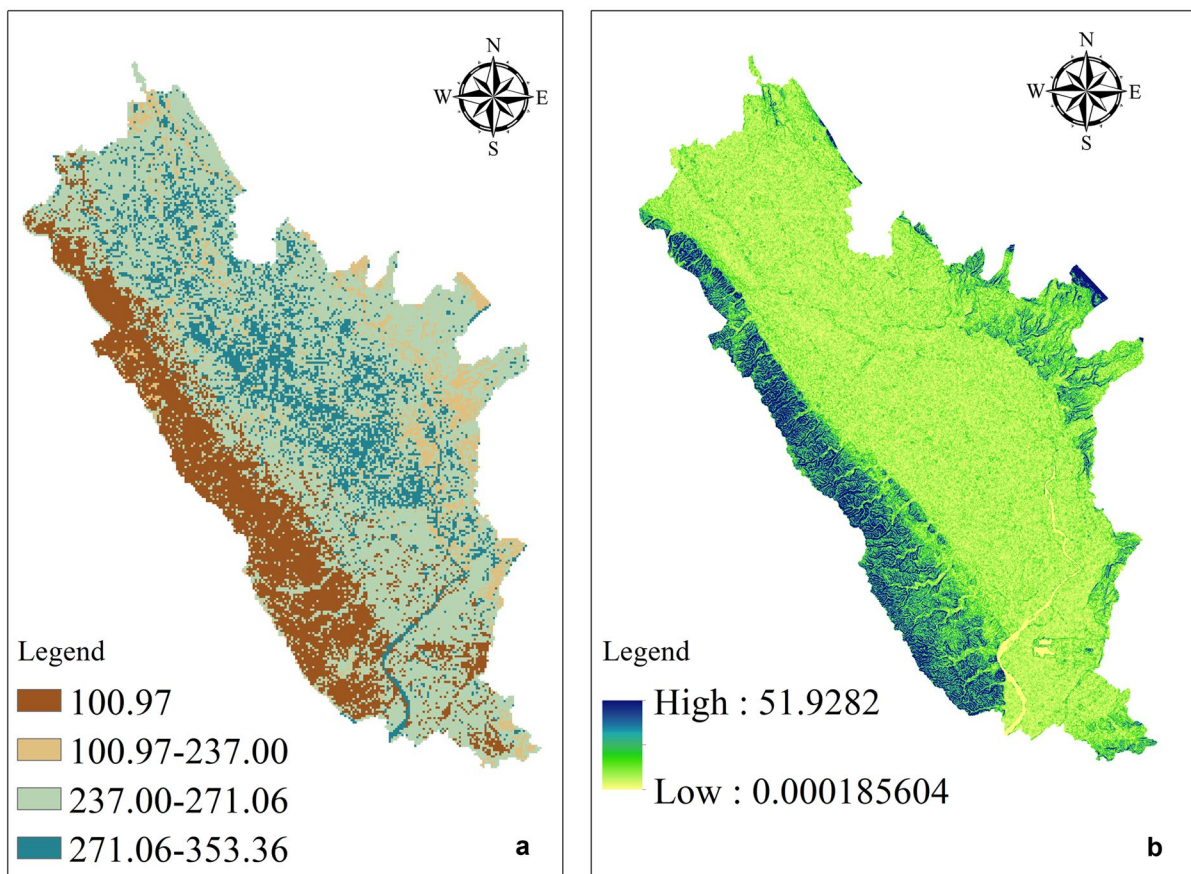
Fig. 5 **a** Estimated runoff (in mm) map of Rupnagar watershed for 18 August 2019. **b** Slope map for Rupnagar watershed

RUN-OFF Vs RAIN-FALL 18/08/2019

$$y = 0.87938x + 31.587$$
$$R^2 = 0.9362$$

Fig. 6 Correlative plots for runoff vs rainfall for 18 August 2019 for Rupnagar (Punjab), India

well submerged underwater leading to loss of coherence. Based on coherence thresholding, since coherence varies from 0 to 1 (1 for persistent scatterers), a flood map was prepared for 6, 18, and 31 August 2019 for Rupnagar (coherence threshold value = 0.2, higher than this were masked out). The flood mask was overlaid on Google earth to understand and visualize the scenario better. The flood inundation map is shown in Fig. 4d.

Results and discussion

Results

The surface runoff, especially in urban areas, depends on many factors like the soil properties, retention capacity, texture of the soil, and the LULC of the target area. Most of the studies that used the SCS-CN method for runoff modeling use optical data that has often cloud cover constraints in monsoon months; using entirely remotely sensed SAR data gives better temporal data availability. Moreover, coherence-based thresholding for flood mapping is another way in which SAR remote sensing has been phenomenally successful. As explained in the previous section, a runoff map was prepared based on the estimated runoff. The minimum runoff was estimated to be 100.97 mm, and the maximum runoff was 353.68 mm on 18 August 2019, as shown in Fig. 5a.

The correlation between rainfall in mm and runoff in mm for August 2019 in Rupnagar is shown in Fig. 6.

Figure 6 shows that due to flash floods in Himachal Pradesh on 18 August 2019, the runoff increased abruptly bearing a high correlation with

the rainfall that occurred on that day. The plot was prepared by plotting runoff vs rainfall and correlating the two. The results showed a high R^2 statistics of 0.93. The rainfall data was acquired on 15 min interval for 7 h and 30 min from the CHRS data portal, and runoff was calculated using the SCS-CN method. It showed that heavy rainfall, cloud burst, and flash floods that occurred in the upper reaches of the Himalayas accumulated into causing a high surface runoff in the Rupnagar watershed and led to submergence of large chunks of agricultural lands and human settlements, calculated to be around 250 km^2. It caused the displacement of many people from their homes who were forced to take shelter in the upper reaches less affected by floods.

Discussion

SAR remote sensing with its high temporal resolution, all-weather data availability, and high spatial resolution, effectively and efficiently helps in high-resolution DEM generation and flood inundation mapping and surface runoff estimation modelling. From this study, it was found that the higher the CN value, the higher is the runoff. When there are floods with an average amount of rainfall, the causes often lie elsewhere as in the areas mentioned above. The areas near the Indian Institute of Technology transit campus and main campus were found to have high flooding potential owing to high CN values. The maximum runoff approximating to 350 mm was found in and around the two campuses of IIT Ropar in Rupnagar, as shown by the runoff map (Fig. 5a) for 18 August 2019, when flooding was at its peak. The SCS-CN method, due to its simplicity, predictability, and based on one parameter approach, is highly responsive to major runoff producing watershed properties. Making use of the soil type, LULC, surface condition, and antecedent moisture condition. The SCS-CN method does not take time factor into account and neither the intensity of rainfall nor its distribution spatially. However, the hydrological findings can be used to plan and develop water resources and reservoirs at the watershed level, for areas with high rainfall and less number of rainy days.

Conclusions

This study utilizes dual polarised SAR data from Sentinel-1A for DEM generation and coherence-based flood inundation mapping. Both studies use SAR interferometry, which has seen wide applications in displacement and subsidence mapping research. The study shows that a higher resolution DEM can be obtained using InSAR and it can be used for effective and accurate runoff modeling.

From the study, the following inferences can be drawn-

- At areas located on high slopes, the runoff is lowest as the water quickly tends to rush down, evident from Fig. 5a, b.
- In previous areas and areas without vegetation cover, the runoff is low due to high water penetration through the surface.
- On comparing the runoff map with Table 1, it was inferred that the maximum amount of runoff is generated in built-up areas and areas with a good amount of vegetation and for areas where there is an abrupt change in slope.

The novelties of this study include:

- This study relies entirely on SAR data and uses a 15 m spatial resolution DEM generated using SAR interferometry, unlike 30 m DEMs generated from optical stereo-pair datasets.
- This study is cost-effective as it utilizes freely available SAR datasets from Sentinel-1A.
- It has high applicability for mapping of flood-prone areas in planning exercises to shift the existing populations to safer places before the onset of monsoons as it can easily delineate the high-risk areas.
- It shows the applicability of the SCS-CN method with SAR data.

Declarations

References

Abdeldayem, O. M., Eldaghar, O., Mostafa, M. K., Habashy, M. M., Hassan, A., Mahmoud, H., & Peters, R. W. (2020). Mitigation plan and water harvesting of flashflood in arid rural communities using modeling approach: A case study in Afouna village. *Egypt. MDPI Water, 12*(9), 1–24. https://doi.org/10.3390/W12092565.

Ahluwalia, R. S., Rai, S. P., Gupta, A. K., Dobhal, D. P., Tiwari, R. K., Garg, P. K., & Kesharwani, K. (2016). Towards the understanding of the flash flood through isotope approach in Kedarnath valley in June 2013, Central Himalaya, India. *Natural Hazards, 82*(1), 321–332. https://doi.org/10.1007/s11069-016-2203-6.

Alexander, L. V., & Arblaster, J. M. (2009). Assessing trends in observed and modelled climate extremes over Australia in relation to future projections. *International Journal of Climatology, 29*(3), 417–435. https://doi.org/10.1002/joc.1730.

Amutha, R., & Porchelvan, P. (2009). Estimation of surface runoff in Malattar sub-watershed using SCS-CN method. *Journal of the Indian Society of Remote Sensing, 37*(2), 291. https://doi.org/10.1007/s12524-009-0017-7.

Behzad, A., Sarvati, M., & Moghimi, E. (2012). Estimating flood potentia l emphasizing on Geomorphologic characteristics in Tarikn Basin using the SC S method. *European Journal of Experimental Biology, 2*(5), 1928–1935.

Bézy, J., Sierk, B., Caron, J., Veihelmann, B., Martin, D., Langen, J., & Zhu, A. G. N. (2014). The Copernicus Sentinel-5 mission for operational atmospheric monitoring : Status and developments. *SPIE Remote Sensing, 9241,* 1–11. https://doi.org/10.1117/12.2068177.

Boerner, W. M. (2007). Recent advancements of radar remote sensing; air- and space-borne multimodal SAR remote sensing in forestry, Agriculture, Geology, Geophysics (Volcanology and Technology): Advances in P0L-SAR, IN-SAR, POLinSAR and POL-DIFF-IN-SAR Sensing and Ima. *2007 Asia-Pacific Microwave Conference.* https://doi.org/10.1109/APMC.2007.4555164.

Borah, S. B., Sivasankar, T., Ramya, M. N. S., & Raju, P. L. N. (2018). Flood inundation mapping and monitoring in Kaziranga National Park, Assam using Sentinel-1 SAR data. *Environmental Monitoring and Assessment, 190*(9), 520. https://doi.org/10.1007/s10661-018-6893-y.

Boughton, W. C. (1989). A review of the USDA SCS curve number method. *Soil Research, 27*(3), 511–523. https://doi.org/10.1071/SR9890511.

Bronstert, A. (2003). Floods and Climate Change: Interactions and Impacts. *Risk Analysis*, *23*(3), 545–557. https://doi.org/10.1111/1539-6924.00335.

Cheng, Q., Ko, C., Yuan, Y., Ge, Y., & Zhang, S. (2006). GIS modeling for predicting river runoff volume in ungauged drainages in the Greater Toronto Area. *Canada. Computers & geosciences, 32*(8), 1108–1119. https://doi.org/10.1016/j.cageo.2006.02.005.

Chini, M., Pelich, R., Pulvirenti, L., Pierdicca, N., Hostache, R., & Matgen, P. (2019). Sentinel-1 InSAR coherence to detect floodwater in urban areas: Houston and hurricane Harvey as a test case. *Remote Sensing, 11*(2), 1–20. https://doi.org/10.3390/rs11020107.

Chung, H. W., Liu, C. C., Cheng, I. F., Lee, Y. R., & Shieh, M. C. (2015). Rapid response to a typhoon-induced flood with an SAR-derived map of inundated areas: Case study and validation. *Remote Sensing, 7*(9), 11954–11973. https://doi.org/10.3390/rs70911954.

Clauss, K., Ottinger, M., & Kuenzer, C. (2018). Mapping rice areas with Sentinel-1 time series and superpixel segmentation. *International Journal of Remote Sensing, 39*(5), 1399–1420. https://doi.org/10.1080/01431161.2017.1404162.

Cosgrove, W. J., & Loucks, D. P. (2015). Water management: Current and future challenges and research directions. *Water Resources Research, 51*(6), 4823–4839. https://doi.org/10.1002/2014WR016869.

Damodaran, H. (2008). The Paradox of Northern Farming Communities BT - India's New Capitalists: Caste, Business, and Industry in a Modern Nation. In H. Damodaran (Ed.) (pp. 259–296). London: Palgrave Macmillan UK. https://doi.org/10.1057/9780230594128_8.

Dongchen, E., Zhou, C., & Liao, M. (2004). Application of SAR Interferometry on DEM Generation of the Grove Mountains. *Photogrammetric Engineering & Remote Sensing*, *70*(10), 1145–1149. https://doi.org/10.14358/PERS.70.10.1145.

Frederick, S. E., Cebula, R. P., & Heath, D. F. (1986). Instrument characterization for the detection of long-term changes in stratospheric ozone: An analysis of the SBUY/2 radiometer. *Journal of Atmospheric and Oceanic Technology, 3*(3), 472–480. https://doi.org/10.1175/1520-0426(1986)003%3c0472:ICFTDO%3e2.0.CO;2.

Geetha, K., Mishra, S. K., Eldho, T. I., Rastogi, A. K., & Pandey, R. P. (2008). SCS-CN-based continuous simulation model for hydrologic forecasting. *Water Resources Management, 22*(2), 165–190. https://doi.org/10.1007/s11269-006-9149-5.

Geetha, M., & Rastogi, & Pandey. . (2007). Modifications to SCS-CN method for long-term hydrologic simulation. *Journal of Irrigation and Drainage Engineering, 133*(5), 475–486. https://doi.org/10.1061/(ASCE)0733-9437(2007)133:5(475).

Grandin, R., Klein, E., Métois, M., & Vigny, C. (2016). Three-dimensional displacement field of the 2015 Mw8.3 Illapel earthquake (Chile) from across- and along-track Sentinel-1 TOPS interferometry. *Geophysical Research Letters, 43*(6), 2552–2561. https://doi.org/10.1002/2016GL067954.

Gupta, S., Javed, A., & Datt, D. (2003). Economics of flood protection in India BT - flood problem and management in South Asia. In M. M. Q. Mirza, A. Dixit, & A. Nishat (Eds.) (pp. 199–210). Dordrecht: Springer Netherlands. https://doi.org/10.1007/978-94-017-0137-2_10.

Heino, R., Brázdil, R., Forland, E., Tuomenvirta, H., Alexandersson, H., Beniston, M., & Wibig, J. (1999). Progress in the study of climatic extremes in northern and central Europe. *Climatic Change, 42*(1), 151–181. https://doi.org/10.1023/A:1005420400462.

Hoomehr, S., Schwartz, J. S., Yoder, D. C., Drumm, E. C., & Wright, W. (2013). Curve numbers for low-compaction steep-sloped reclaimed mine lands in the Southern Appalachians. *Journal of Hydrologic Engineering, 18*(12), 1627–1638. https://doi.org/10.1061/(ASCE)HE.1943-5584.0000746.

Hughes, L. (2000). Biological consequences of global warming: Is the signal already apparent? *Trends in Ecology & Evolution, 15*(2), 56–61. https://doi.org/10.1016/S0169-5347(99)01764-4.

Jayraman, V., Chandrasekhar, M., & Rao, U. (1997). Managing the natural disasters from space technology inputs. *Acta Astronautica, 40*(2), 291–325. https://doi.org/10.1016/S0094-5765(97)00101-X.

Jung, J., Kim, D., Member, S., Lavalle, M., & Yun, S. (2016). Coherent change detection using InSAR temporal decorrelation model: A case study for volcanic ash detection. *IEEE Transactions on Geoscience and Remote Sensing, 54*(10), 5765–5775. https://doi.org/10.1109/TGRS.2016.2572166.

Kadam, A. K., Kale, S. S., Pande, N. N., Pawar, N. J., & Sankhua, R. N. (2012). Identifying potential rainwater harvesting sites of a semi-arid, basaltic region of Western India Using SCS-CN Method. *Water Resources Management, 26*(9), 2537–2554. https://doi.org/10.1007/s11269-012-0031-3.

Kale, V. S., Ely, L. L., Enzel, Y., & Baker, V. R. (1994). Geomorphic and hydrologic aspects of monsoon floods on the Narmada and Tapi Rivers in central India. *Geomorphology and Natural Hazards: Proceedings of the 25th Binghamton Symposium in Geomorphology, Held 24th September–25,1994 at SUNY, Binghamton, USA, 10*, 157–168. https://doi.org/10.1016/B978-0-444-82012-9.50015-3.

Katimon, A., Zulkifli, M., & Yunos, M. (2003). Flood potential estimation of two small vegetated watersheds. *Malaysian Journal of Civil Engineering, 15*(1), 1–15. https://doi.org/10.11113/mjce.v15.103.

Kuenzer, C., Bluemel, A., Gebhardt, S., Quoc, T. V., & Dech, S. (2011). *Remote sensing of mangrove ecosystems: A review. Remote Sensing* (Vol. 3). https://doi.org/10.3390/rs3050878.

Kuenzer, C., Guo, H., Huth, J., Leinenkugel, P., Li, X., & Dech, S. (2013). Flood mapping and flood dynamics of the mekong delta: ENVISAT-ASAR-WSM based time series analyses. *Remote Sensing, 5*(2), 687–715. https://doi.org/10.3390/rs5020687.

Kumar, A., Gupta, A. K., Bhambri, R., Verma, A., Tiwari, S. K., & Asthana, A. K. L. (2018). Assessment and review of hydrometeorological aspects for cloudburst and flash flood events in the third pole region (Indian Himalaya). *Polar Science, 18,* 5–20. https://doi.org/10.1016/j.polar.2018.08.004.

Lanari, R., Fornaro, G., Riccio, D., Migliaccio, M., Papathanassiou, K. P., Moreira, J. R., & Coltelli, M. (1996). Generation of digital elevation models by using SIR-C/X-SAR multifrequency two-pass interferometry: the Etna case study. *IEEE Transactions on Geoscience and Remote Sensing, 34*(5), 1097–1114. https://doi.org/10.1109/36.536526.

Latha, M., Rajendran, M., & Murugappan, A. (2012). Comparison of GIS-based SCS-CN and Strange table Method of Rainfall-Runoff Models for. *International Journal of Scientific & Engineering Research, 3*(10), 3–7. Retrieved from https://www.ijser.org/paper/Comparison-of-GIS-based-SCS-CN-and-Strange-table-Method-of-Rainfall-Runoff.html.

Lloyd, G. E. (1987). Atomic number and crystallographic contrast images with the SEM: a review of backscattered electron techniques. *Mineralogical Magazine, 51*(359), 3–19. https://doi.org/10.1180/minmag.1987.051.359.02.

Mishra, S. K., Jain, M. K., & Singh, V. P. (2004). Evaluation of the SCS-CN-based model incorporating antecedent moisture. *Water Resources Management, 18*(6), 567–589. https://doi.org/10.1007/s11269-004-8765-1.

Mishra, S. K., & Singh, V. P. (1999). Another look at SCS-CN method. *Journal of Hydrologic Engineering, 4*(3), 257–264. https://doi.org/10.1061/(ASCE)1084-0699(1999)4:3(257).

Mishra, S. K., & Singh, V. P. (2004). Validity and extension of the SCS-CN method for computing infiltration and rainfall-excess rates. *Hydrological processes, 18*(17), 3323–3345. https://doi.org/10.1002/hyp.1223.

Mishra, S. K., Pandey, R. P., Jain, M. K., & Singh, V. P. (2008). A rain duration and modified AMC-dependent SCS-CN procedure for long duration rainfall-runoff events. *Water Resources Management, 22*(7), 861–876. https://doi.org/10.1007/s11269-007-9196-6.

Mishra, S., Mazumdar, S., & Suar, D. (2010). Place attachment and flood preparedness. *Journal of Environmental Psychology, 30*(2), 187–197. https://doi.org/10.1016/j.jenvp.2009.11.005.

Murmu, P., Kumar, M., Lal, D., Sonker, I., & Kumar, S. (2019). Groundwater for Sustainable Development Delineation of groundwater potential zones using geospatial techniques and analytical hierarchy process in Dumka district , Jharkhand , India. *Groundwater for Sustainable Development, 9*(October 2018), 100239. https://doi.org/10.1016/j.gsd.2019.100239.

Naab, F. Z., Dinye, R. D., & Kasanga, R. K. (2013). Urbanization and its impact on agricultural lands in growing cities in developing countries: a case study of Tamale in Ghana. *Modern Social Science Journal, 2*(2), 256–287.

Nishida, K., Nemani, R. R., Glassy, J. M., & Running, S. W. (2003). Development of an evapotranspiration index from Aqua/MODIS for monitoring surface moisture status. *IEEE Transactions on Geoscience and Remote Sensing, 41*(2), 493–501. https://doi.org/10.1109/TGRS.2003.811744.

Pandit, A., & Heck, H. H. (2009). Estimations of soil conservation service curve numbers for concrete and asphalt. *Journal of Hydrologic Engineering, 14*(4), 335–345. https://doi.org/10.1061/(ASCE)1084-0699(2009)14:4(335).

Peters, G., McCall, M. K., & Westen, C. (2012). Coping strategies and risk manageability: using participatory geographical information systems to represent local knowledge. *Disasters, 36*(1), 1–27. https://doi.org/10.1111/j.1467-7717.2011.01247.x.

Phalkey, R., Dash, S., Mukhopadhyay, A., Runge-Ranzinger, S., & Marx, M. (2012). Prepared to react? Assessing the functional capacity of the primary health care system in rural Orissa, India to respond to the devastating flood of September 2008. *Global Health Action, 5*(1), 10964. https://doi.org/10.3402/gha.v5i0.10964.

Ramakrishnan, D., Bandyopadhyay, A., & Kusuma, K. N. (2009). SCS-CN and GIS-based approach for identifying potential water harvesting sites in the Kali Watershed, Mahi River Basin, India. *Journal of Earth System Science, 118*(4), 355–368. https://doi.org/10.1007/s12040-009-0034-5.

Revi, A. (2008). Climate change risk: An adaptation and mitigation agenda for Indian cities. *Environment and Urbanization, 20*(1), 207–229. https://doi.org/10.1177/0956247808089157.

Saini, P., Saini, P., Kaur, J. J., Francies, R. M., Gani, M., Rajendra, A. A., & Chauhan, S. S. (2020). Molecular approaches for harvesting natural diversity for crop improvement BT

- Rediscovery of genetic and genomic resources for future food security. In R. K. Salgotra & S. M. Zargar (Eds.) (pp. 67–169). Singapore: *Springer Singapore*. https://doi.org/10.1007/978-981-15-0156-2_3.

Sandwell, D. T., & Price, E. J. (1998). Phase gradient approach to stacking interferograms. *Journal of Geophysical Research: Solid Earth, 103*(B12), 30183–30204. https://doi.org/10.1029/1998JB900008.

Sanyal, J., & Lu, X. X. (2004). Application of remote sensing in flood management with special reference to Monsoon Asia: A review. *Natural Hazards, 33*(2), 283–301. https://doi.org/10.1023/B:NHAZ.0000037035.65105.95.

Sanyal, J., & Lu, X. X. (2005). Remote sensing and GIS-based flood vulnerability assessment of human settlements: a case study of Gangetic West Bengal, India. *Hydrological Processes, 19*(18), 3699–3716. https://doi.org/10.1002/hyp.5852.

Satheeshkumar, S., Venkateswaran, S., & Kannan, R. (2017). Rainfall–run-off estimation using SCS–CN and GIS approach in the Pappiredipatti watershed of the Vaniyar sub-basin, South India. *Modeling Earth Systems and Environment, 3*(1), 1–8. https://doi.org/10.1007/s40808-017-0301-4.

Schwartz, S. S. (2010). Effective curve number and hydrologic design of pervious concrete storm-water systems. *Journal of Hydrologic Engineering, 15*(6), 465–474. https://doi.org/10.1061/(ASCE)HE.1943-5584.0000140.

Sharma, S. B., & Singh, A. K. (2014). Assessment of the flood potential on a lower Tapi basin tributary using SCS-CN method integrated with remote sensing & GIS data. *Journal of Geography & Natural Disasters, 4*(2), 1–7. https://doi.org/10.4172/2167-0587.1000128.

Sharma, S., & Singh, A. (2015). Assessment of the flood potential on a lower tapi basin tributary using SCS- CN method integrated with remote sensing & GIS data. *Journal of Geography & Natural Disasters*, (August 2014). https://doi.org/10.4172/2167-0587.1000128.

Shen, X., Wang, D., Mao, K., Anagnostou, E., & Hong, Y. (2019). Inundation extent mapping by synthetic aperture radar: A review. *Remote Sensing, 11*(7), 1–17. https://doi.org/10.3390/RS11070879.

Sivakumar, M. V. K. (2007). Interactions between climate and desertification. *Agricultural and Forest Meteorology, 142*(2), 143–155. https://doi.org/10.1016/j.agrformet.2006.03.025.

Small, D., Pasquali, P., & Fuglistaler, S. (1996). A comparison of phase to height conversion methods for SAR interferometry. In *IGARSS '96. 1996 International Geoscience and Remote Sensing Symposium* (Vol. 1, pp. 342–344 vol.1). https://doi.org/10.1109/IGARSS.1996.516334.

Soulis, K. X., & Valiantzas, J. D. (2012). SCS-CN parameter determination using rainfall-runoff data in heterogeneous watersheds – the two-CN system approach. *Hydrology and Earth System Sciences, 16*(3), 1001–1015. https://doi.org/10.5194/hess-16-1001-2012.

Tapete, D. (2018). Appraisal of opportunities and perspectives for the systematic condition assessment of heritage sites with copernicus Sentinel-2 high-resolution multispectral imagery. *MDPI Remote Sensing*, 1–22. https://doi.org/10.3390/rs10040561.

Tripathi, A., & Kumar, S. (2019). Effect of phase filtering on interferometry based displacement analysis of cultural heritage sites. In *2018 5th IEEE Uttar Pradesh Section International Conference on Electrical, Electronics and Computer Engineering (UPCON)* (pp. 1–5). IEEE. https://doi.org/10.1109/UPCON.2018.8597027.

Tripathi, A., & Tiwari, R. K. (2019 a). C-band SAR Interferometry based flood inundation mapping for Gorakhpur and adjoining areas. In 2019 *International Conference on Computer, Electrical & Communication Engineering (ICCECE)* (pp. 1–6). https://doi.org/10.1109/ICCECE44727.2019.9001870.

Tripathi, A., & Tiwari, R. K. (2019 b). Utilization of space-borne C-band SAR data for analysis of flood impact on agriculture and its management. *International Archives of the Photogrammetry, Remote Sensing and Spatial Information Sciences*, 42(3/W6). https://doi.org/10.5194/isprs-archives-XLII-3-W6-521-2019.

Tripathi, A., & Tiwari, R. K. (2019 c). Mapping of deflection caused due to hydrostatic pressure using Differential SAR Interferometry (DInSAR) on Bhakhra dam. *IEEE XPLORE*. https://doi.org/10.1109/UPCON47278.2019.8980117.

Tripathi, A., & Tiwari, R. K. (2020). Synergetic utilization of sentinel-1 SAR and sentinel-2 optical remote sensing data for surface soil moisture estimation for Rupnagar, Punjab, India. *Geocarto International*, 1–22. https://doi.org/10.1080/10106049.2020.1815865.

Tsai, Y. L. S., Dietz, A., Oppelt, N., & Kuenzer, C. (2019). Remote sensing of snow cover using spaceborne SAR: A review. *Remote Sensing*, 11(12). https://doi.org/10.3390/rs11121456.

Wałęga, A., & Rutkowska, A. (2015). Usefulness of the modified NRCS-CN method for the assessment of direct runoff in a mountain catchment. *Acta Geophysica, 63*(5), 1423–1446. https://doi.org/10.1515/acgeo-2015-0043.

Wright, R. (2009). The Ancient Indus - Urbanism, Economy and Society. In *Ancient Pakistan* (Vol. XX, p. 2009). Retrieved from http://journals.uop.edu.pk/papers/AP_v20_249to249.pdf.

Xu, F., & Jin, Y. (2007). Automatic reconstruction of building objects from multiaspect meter-resolution SAR images. *IEEE Transactions on Geoscience and Remote Sensing, 45*(7), 2336–2353. https://doi.org/10.1109/TGRS.2007.896614.

Zhang, M., Chen, F., Liang, D., Tian, B., & Yang, A. (2020). Use of sentinel-1 grd SAR images to delineate flood extent in Pakistan. *Sustainability (Switzerland), 12*(14), 1–19. https://doi.org/10.3390/su12145784.

Zhu, L., Suomalainen, J., Liu, J., Hyyppä, J., Kaartinen, H., & Haggren, H. (2018). A review: remote sensing sensors. *Multi-purposeful application of geospatial data*, 19-42. https://doi.org/10.5772/intechopen.71049.